Nanoscale

COMMUNICATION

View Article Online
View Journal | View Issue



Cite this: *Nanoscale*, 2015, **7**, 17268

Received 3rd May 2015,
Accepted 14th September 2015

DOI: 10.1039/c5nr02876k

www.rsc.org/nanoscale

# Fabrication of ultra-thin silicon nanowire arrays using ion beam assisted chemical etching†

Zhiyuan Tan, Wenjia Shi, Chungang Guo, Quan Zhang, Liang Yang, Xiaoling Wu, Guo-an Cheng and Ruiting Zheng*

**Uniform dispersion of Au–Ag alloy nanoparticles underneath the surface of a Si wafer is realized *via* Au film pre-deposition and Ag ion implantation. The Au–Ag nanoparticles are used as catalysts in metal assisted chemical etching for fabricating Si nanowire arrays with average diameters of less than 10 nm. We find that the alloy catalysts introduced by ion implantation are the key to obtaining thin nanowire arrays and we also demonstrate that SiNWAs with various diameters could be simply produced by changing the thickness of the pre-deposited Au layer. Compared with the traditional process, ion beam assisted chemical etching is proven to be a convenient and efficient approach to fabricate ultra-thin SiNWAs on a large scale.**

Owing to their excellent biocompatibility and unique electrical, optical, magnetic, and thermal properties, silicon nanowire arrays (SiNWAs) have potential applications in cell capture,[1–3] Li-batteries,[4,5] thermoelectric devices,[6–8] and photovoltaic cells.[9–11] Numerous approaches such as vapor–liquid–solid (VLS) growth,[12,13] thermal-evaporation oxide-assisted growth[14] and metal-assisted chemical etching (MACE)[15–17] have been developed to fabricate SiNWAs. In recent years, ultra-thin Si nanowires are of great interest to researchers. It was reported that Si nanowires with diameters smaller than 1.14 nm will turn from indirect-gap semiconductors into direct-gap semiconductors,[18] and porous Si nanowires with nanoparticles smaller than 4 nm will show strong visible photoluminescence.[19] Besides, the SiNWAs with smaller diameters showed lower thermal conductivities and a much better thermoelectric performance.[20] It was also found that thin Si nanowires would avoid fracture during recharge cycles, which is important for their application in Li-ion batteries.[21]

Due to the long-standing demand for thin SiNWAs, many efforts have hence been devoted to synthesize SiNWAs with small diameters. Ultra-thin SiNWs with diameters of less than 10 nm were produced using a vapor–liquid–solid (VLS) method.[12] However, the growth direction of SiNWs is dependent on their diameters, and vertical ultra-thin SiNWAs with specific orientations may not be realized by this method. Surface patterning combined with metal-assisted chemical etching,[22] size reduction lithography[23] and reactive ion etching[24] were also applied to achieve silicon nanowire arrays with diameters down to sub-10 nm. In these approaches, prepared masks, lithography or other methods are needed. These extra procedures are time and money consuming, and limit the possibility of large-scale fabrication.

Compared with the other methods, MACE is a simple and effective method.[25] However, the average diameters of silicon nanowires achieved using MACE are always larger than one hundred nanometers.[26,27] There are two reasons that prevent MACE from achieving thin Si nanowires. First, silver is the most commonly used metal catalyst in MACE because of its lower cost and better performance compared to other catalysts. However, Ag catalysts deposited on silicon are usually dozens or hundreds of nanometers in diameter, it is hard to achieve several nanometer gaps using these catalysts,[28,29] and the gaps decide the diameters of the Si nanowires in the following etching process. Moreover, during the etching process, the Ag particles will grow up due to Ostwald ripening,[15,30] which will make the diameter of the SiNWAs even larger and non-uniform.

In this work, we report a novel ion beam assisted chemical etching (IBCE) method to produce ultra-thin silicon nanowire arrays. Different from the traditional MACE, ion implantation is employed to disperse Au–Ag alloy catalysts into the silicon wafer, which will largely reduce the size of the catalysts. We find that the alloy catalysts introduced by ion implantation could avoid Ostwald ripening during the following chemical etching process. Using this method, a large quantity of ultra-thin SiNWAs could be fabricated conveniently, efficiently and cheaply.

Fig. 1 shows the schematic diagram of the IBCE process. First, a thin Au film is deposited on the surface of a Si wafer,

*Key Laboratory of Radiation Beam Technology and Materials Modification of Ministry of Education, College of Nuclear Science and Technology, Beijing Normal University, Beijing 100875, China. E-mail: rtzheng@bnu.edu.cn*

†Electronic supplementary information (ESI) available. See DOI: 10.1039/c5nr02876k

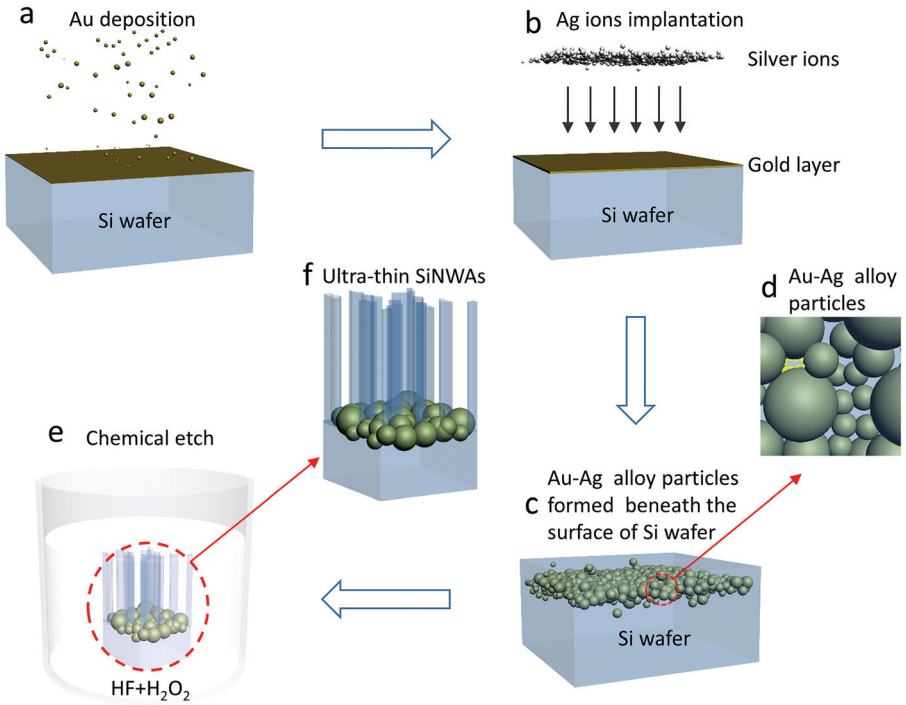


**Fig. 1** Schematic diagram of the IBCE process. (a) A thin gold layer is deposited on the surface of a Si wafer. (b) Ag ions are implanted into the sample. (c) Small Au–Ag alloy particles are formed beneath the surface of the Si wafer. (d) Top view of a magnified picture of Au–Ag alloy particles, the yellow dashed line denotes the gaps between the alloy particles. (e) The samples are etched in HF/$H_2O_2$ solutions. (f) The thin SiNWAs achieved by this method.

as shown in Fig. 1a. After that, the Ag ions are implanted into the samples (Fig. 1b). At room temperature and at an appropriate dose, large quantities of Au–Ag particles are formed beneath the surface of the Si wafer, as indicated by Fig. 1c. These particles will act as the catalysts in the following chemical etching process. As shown in the cross-sectional TEM image (ESI Fig. S1†), the alloy particles formed beneath the surface of the Si wafer are distributed in three dimensions, which is apparently different from the two-dimensional distribution of catalysts in the traditional MACE. The three dimensional distribution of the metal particles leads to the overlap of the catalysts on the projection plane (perpendicular to the implanting direction), which forms lots of tiny gaps between the small particles on the projection plane, as indicated by the yellow dashed line in Fig. 1d. These gaps will evolve into Si nanowires during the following etching process (Fig. 1e). When the implanted samples were etched in $H_2O_2$/HF mixed solutions, thin silicon wire arrays were obtained (Fig. 1f). The length of the Si nanowires depends on the etching times, the diameter and the density of the Si nanowires are defined by the size and density of the inter-particle gaps on the projection plane.

Fig. 2 shows the Si nanowire arrays obtained *via* a typical IBCE process, *i.e.*, pre-deposit a 6 nm Au layer on a Si (100) wafer and then implant the Au-coated Si wafer with 30 kV of Ag ions at a dose of $5 \times 10^{16}$ ions per $cm^2$. After that the wafer is immersed into an $H_2O_2$/HF mixed solution (30 wt% $H_2O_2$ : 40 wt%HF : $H_2O$ = 1 : 12 : 37 (vol%)) to etch for 40 min. Fig. 2a and b show the SEM image of the top view and the side view of the as-prepared NWAs, respectively. The top of the nanowires aggregate together and look like lodging wheat, which may be due to the large surface tension of the aqueous solution and the small rigidity of the ultra-thin nanowires. From Fig. 2b, we can observe that the height of the array is about 9.6 μm. The diameters of the nanowires are uniform, which is apparently different from the SiNWAs achieved *via* traditional MACE.[27–29] High resolution SEM (Fig. 2c) reveals that the diameters of most nanowires are distributed between 6 nm and 12 nm, as the inset in Fig. 2c shows. The TEM image (Fig. S2 in ESI†) shows some individual nanowires and the SiNWs have a uniform diameter distribution. The average diameter of the nanowires is about 9.3 nm, which indicates that the SiNWAs have an aspect ratio larger than 1000. Fig. 2d is a high resolution TEM image of a Si nanowire. The diameter of the nanowire is about 7 nm. The single crystal silicon core is covered by an amorphous shell with a thickness of 0.5 nm. The lattice distance indicates that the axial direction of the nanowire is <100>, which is consistent with the orientation of the Si wafer.

A pre-deposited Au layer is important for producing thin Si nanowires. Fig. 3a shows the typical microstructure of the Ag implanted blank silicon wafer. From the high resolution TEM image (the inset of Fig. 2a), we can find that the dark area shows a crystalline structure, and the d-spacing of 0.205 nm is

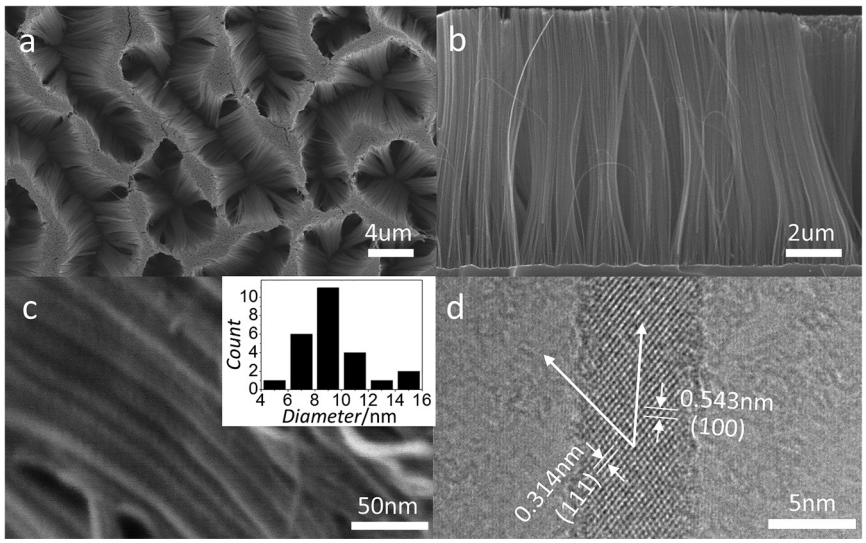


**Fig. 2** (a) A top view SEM image of the ultra-thin SiNWAs fabricated using IBCE. (b) The cross-sectional SEM image of the ultra-thin SiNWAs. (c) A higher magnification SEM image of the SiNWAs. The inset shows the diameter distribution of these SiNWAs. (d) A HR-TEM image of a SiNW obtained using IBCE.

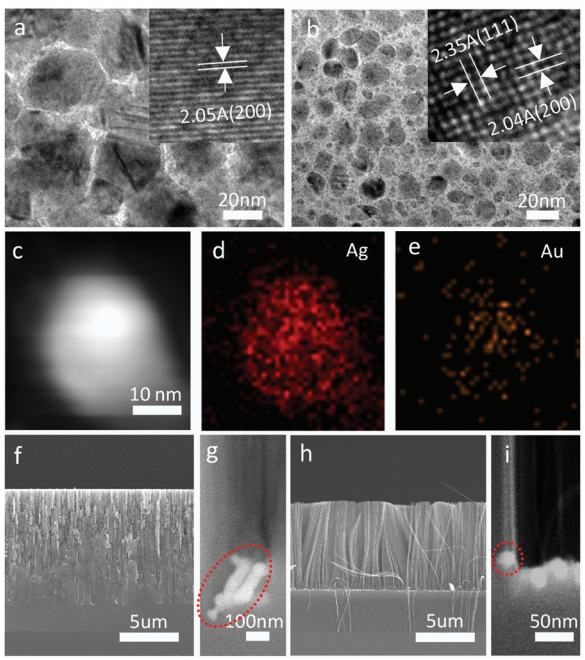


**Fig. 3** Effect of the pre-deposited Au layer on the morphology of the Si nanowire arrays. (a) TEM image of the catalysts that were formed by implanting Ag ions into a blank Si wafer. The inset is a lattice image of an Ag particle. (b) TEM image of the catalysts that were formed by implanting Ag ions into the Si wafer with a pre-deposited Au layer of 6 nm. The inset is a lattice image of an Au–Ag alloy catalyst. (c) HAADF-STEM image of a nanoparticle in (b). (d) Ag and (e) Au EDS mapping of the particle in (c). (f) SEM images of the Si nanostructure obtained by implanting Ag ions on a blank Si wafer and etched in an $HF/H_2O_2$ mixed solution for 40 min. (g) SEM images of the catalyst morphology in (f). (h) SEM images of the SiNWAs obtained by implanting Ag ions on the Si wafer with a pre-deposited Au layer of 6 nm and followed by etching in an $HF/H_2O_2$ mixed solution for 40 min. (i) SEM images of the catalyst morphology in (h). The implanted Ag ion dose of all samples is $2.5 \times 10^{16}$ ions per $cm^2$.

close to that of the silver (200) face, suggesting that the particle is made up of silver. The light-colour area between the Ag particles represents the Si substrates. Fig. 3b shows the microstructure of the Au pre-coated silicon wafer implanted with Ag ions. The distances of 0.235 nm and 0.204 nm shown in the inset are very close to the interplanar spacing of (111) and (200) of the Au–Ag alloy, respectively, however it is not sufficient to determine the composition of the particle only with the lattice parameters because the lattice parameters of Au, Ag and their alloys are quite close. We further observe a catalyst particle using HAADF-STEM (high-angle annular dark-field scanning transmission electron microscopy) and EDS mapping. Fig. 3c is the HAADF-STEM image of the particle, Fig. 3d and e are the Ag and Au EDS mapping of the particle, respectively. It can be observed that the particle contains both the Ag and Au elements. The result suggests that the nanoparticles are made up of Au and Ag, which supports our hypothesis that the alloy particle is formed during the process. Between the gaps of the large particles, lots of small alloy particles could be observed (Fig. 3b). Small and stable catalysts are the key to obtaining ultra-thin SiNWAs and we find that a pre-deposited Au layer is important for reducing the size and keeping the stability of the alloy catalysts. The average diameter of the catalyst formed by implanting Ag ions into a blank Si wafer is about 30–40 nm (Fig. 3a), much larger than that formed in the samples with a pre-deposited Au layer, which is only about 10 to 20 nm (Fig. 3b). In IBCE, the energetic Ag ions first collide with the Au atoms and then penetrate into the silicon wafer until the energy is totally consumed. The Au film can consume the kinetic energy of the Ag ions and reduce the migration energy of the Ag atoms in silicon. Furthermore, in the equilibrium state, Ag–Si or Au–Si is not immiscible. The implanted Ag ions tend to form Au–Ag alloys

 

when the Au atoms exist. So Au atoms or clusters could act as nucleation centres for seeding the alloy particles. The adequacy of the nucleation centres can largely reduce the size of the alloy particles, which cannot be realized only by reducing the implantation dose of the Ag ions. To further study the effect of the pre-deposited Au layer, the two samples were etched in an HF/$H_2O_2$ mixed solution (30 wt%$H_2O_2$ : 40 wt% HF : $H_2O$ = 1 : 12 : 37 (vol%)) for 40 min. The achieved Si nanostructures and the morphologies of the catalysts are shown in Fig. 3f–i. For the sample without the Au layer, only porous structures are formed (Fig. 3f), indicating that the Ag ion dose of $2.5 \times 10^{16}$ ions per $cm^2$ is insufficient for fabricating SiNWAs, which may be due to Ostwald ripening of the Ag particles during etching. The disappeared Ag particles would leave hollow pits, whereas the large Ag particles may lead to pores with diameters larger than several hundred nanometers. The direct evidence is clearly shown in Fig. 3g, a 300 nm Ag cluster is formed at the bottom of the large caves, which is about ten times larger than its initial size. In our experience, it's hard to obtain ultra-thin Si nanowires only by Ag ion implantation. In contrast, thin SiNWAs with uniform diameters were well formed on the samples with a 6 nm pre-deposited Au layer (Fig. 3h). The average diameter of the alloy catalysts is about 20 nm (Fig. 3i) after 40 min of etching, indicating that there is no obvious Ostwald ripening for the Au–Ag alloy catalyst. The promising stability of the alloy catalyst may come from the chemical stability of Au. The catalyst keeping its initial state during etching is beneficial for producing SiNWAs with desired shapes and diameters. The length of the nanowires in Fig. 3h is nearly the same as the depth of the nano-pores in Fig. 3f, indicating that the catalytic activity of the Au–Ag alloy is only a bit lower than that of pure Ag. With the help of the Au layer, even a $5 \times 10^{15}$ ions per $cm^2$ dose of Ag ions is sufficient to obtain the SiNWAs (seen Fig. S3 in ESI†). So IBCE can conserve more of the catalysts compared to traditional MACE.

Various diameters of the SiNWAs can be achieved by simply adjusting the thickness of the pre-deposited Au layer in IBCE. Fig. 4 shows the influence of the Au layer thickness on the morphologies of the SiNWAs. In these samples, gold layers with thicknesses of 1, 6, 11 and 16 nm are first sputtered on the surface of the Si wafer. Ag ions with a dose of $5 \times 10^{16}$ ions per $cm^2$ are then implanted into the samples. After that, the samples were etched in an $H_2O_2$/HF mixed solution (30 wt% $H_2O_2$ : 40 wt%HF : $H_2O$ = 1 : 12 : 37 (vol%)) for 40 min. Fig. 4a–d show the SEM images of the SiNWAs with various pre-deposited Au thicknesses. Fig. 4a (a 1 nm Au layer) and Fig. 4d (a 16 nm Au layer) look alike, the SiNWAs are divided into small areas by several big cracks. Fig. 4b (a 6 nm Au layer) and Fig. 4c (an 11 nm Au layer) are similar, the Si nanowires lean against each other and look like lodging wheat. High resolution SEM images indicate that adjoining Si nanostructures are

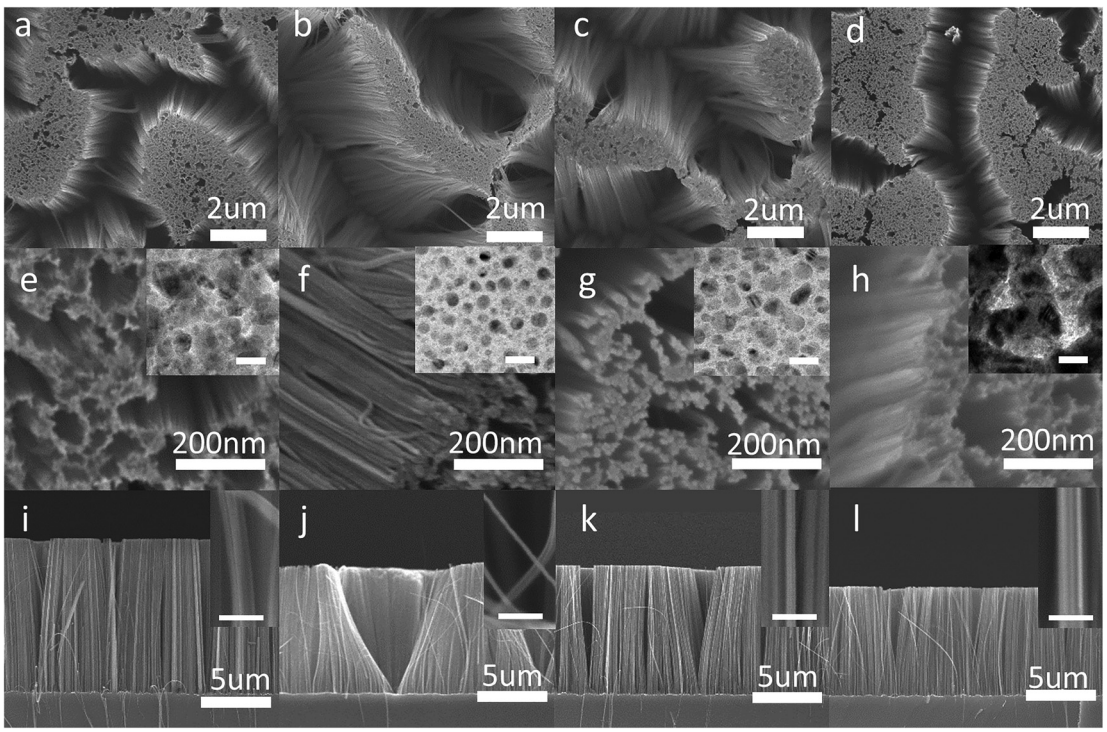


**Fig. 4** Influence of the Au layer thickness on the morphology of the SiNWAs. (a)–(d) The top view SEM images of the SiNWAs obtained with pre-deposited Au layers of 1 nm, 6 nm, 11 nm, and 16 nm, respectively. (e)–(h) The higher magnification SEM of a–d, respectively, the inset TEM image shows the morphology of the alloy catalysts formed after implantation, the scale bar in the inset is 20 nm. (i)–(l) The cross-section image of the SiNWAs obtained with a pre-deposited Au layer of 1 nm, 6 nm, 11 nm, and 16 nm, respectively. The insets show magnified pictures, the scale bar in the inset is 100 nm.

formed on the samples pre-deposited with a 1 nm Au layer (Fig. 4e) and a 16 nm Au layer (Fig. 4h). But the nanowires are separated on the samples pre-deposited with a 6 nm Au layer (Fig. 4f) and an 11 nm Au layer (Fig. 4g). The inset pictures in Fig. 4e–h show that the morphology of the catalyst particles changes as the thickness of the pre-deposited Au layer increases. The large metal clusters (the inset of Fig. 4e) are formed when the thickness of the Au layer is 1 nm, implying that the quantity of Au is insufficient for synthesizing small catalyst particles. With the pre-deposited Au layer increasing to 6 nm, the sizes of the catalysts become much smaller, and well separated alloy particles are obtained (the inset of Fig. 4f). It seems that the separated catalysts will lead to a continuous silicon structure, rather than the individual silicon nanowires after chemical etching. However, the HAADF-STEM image (Fig. S4 in ESI†) shows that the smaller particles between the larger ones are helpful for cutting the large gaps into small pieces and result in a uniform distribution of the separated thin SiNWAs. When the thickness of the Au layer increases to 11 nm, the particles grow larger, but separated catalysts can still be observed in the inset of Fig. 4g. When the thickness of the pre-deposited Au layer reaches 16 nm, the adjoining metal structure (the inset of Fig. 4h) is formed because of the excess Au element. In our experiments, a 6 nm Au layer is appropriate for producing the finest catalyst particles. From the higher magnification cross-section images (the inset of Fig. 4i–l), we can observe that the diameter of the Si nanowires varies with the thickness of the Au layer, which shows a similar trend with the variation of the catalyst size. It proves our conjecture that small catalyst particles are beneficial for synthesizing thin Si nanowires. From Fig. 4i–l, the length of the nanowire arrays decreases with the increase of the gold layer thickness, which may indicate the slight decrease of the catalyst activity. The reason may due to the catalytic activity differences between gold and silver, as we all know, that Si atoms start to dissolve in the $HF/H_2O_2$ mixed solution when $h^+$ is injected into the Si wafer.[15,30] The $h^+$ is provided from the oxidation of the noble metal catalysts. The more negative redox potential of the Ag catalyst makes the oxidation process occur more easily, thus leading to a faster etching speed than for the Au catalyst in MACE. In other words, the catalytic activity of Ag is higher than that of Au in silicon etching. A thicker Au layer will lead to a higher Au content in the alloy particles, which may reduce their catalytic activity. We also investigate the influence of the Ag ion dose on the morphology of the SiNWAs, which shows a similar result (Fig. S5†).

## Conclusions

In summary, ion implantation provides a possibility to precisely control the size of catalyst particles and the diameters of SiNWAs. Au–Ag alloy particles that were made *via* ion implantation are proven to have small sizes, promising catalytic activities and chemical stabilities. The ultra-thin vertical nanowire arrays with average diameters of about 9.3 nm are manufactured using this method. In brief, IBCE is a convenient, cheap, and easy-to-expand method for generating vertical ultra-thin SiNWAs with an excellent crystalline nature, which could be applied in Li-batteries and thermoelectric and photoluminescence devices.

## Experimental methods

For the experiment, an n-type Si (1–0–0) wafer (1–10 Ω) with a thickness of 550 μm was cut into 2 × 2 $cm^2$ pieces. The samples were degreased by respectively rinsing in acetone, ethanol, and deionized water for 5 min and the oxide layer was removed *via* immersion in a dilute HF solution. The Au layers with different thicknesses (1 to 16 nm) were deposited on the samples using a direct-current (DC) sputtering source. The Au deposition rate was fixed at 6.7 nm per min, and the thickness was manipulated by controlling the deposition time. After that, the Ag ions, with an acceleration voltage of 30 kV and a dose between $5 \times 10^{15}$ and $5 \times 10^{17}$ ions per $cm^2$, were implanted into the samples at room temperature. Then the samples were etched in an $H_2O_2$/HF mixed solution (30 wt% $H_2O_2$ : 40 wt%HF : $H_2O$ = 1 : 12 : 37 (vol%)) for 40 min and the products (silicon wire arrays) were obtained and dried in air. SEM (Hitachi S-4800), TEM and HAADF-STEM (FEI Tecnai $G^2$ F20) were used to investigate the morphology of the SiNWAs. To explore the morphology of the catalyst underneath the surface of the Si wafer, we used a free-standing thin Si film with a thickness of 48 nm which was supported by a TEM copper mesh. The gold layers with different thicknesses were deposited on the Si films, and then the samples were implanted with Ag ions.

## Acknowledgements

This work is supported by the National Nature Science Foundation of China (11575025), the Fundamental Research Funds for the Central Universities, Program for New Century Excellent Talents in University (NCET-11-0043) and the National Basic Research Program of China (2010CB832905).

## Notes and references

1 S. Wang, H. Wang, J. Jiao, K. J. Chen, G. E. Owens, K. Kamei, J. Sun, D. J. Sherman, C. P. Behrenbruch, H. Wu and H. R. Tseng, *Angew. Chem., Int. Ed.*, 2009, **48**, 8970–8973.
2 L. Chen, X. Liu, B. Su, J. Li, L. Jiang, D. Han and S. Wang, *Adv. Mater.*, 2011, **23**, 4376–4380.
3 H. E. Jeong, I. Kim, P. Karam, H. J. Choi and P. Yang, *Nano Lett.*, 2013, **13**, 2864–2869.
4 C. K. Chan, H. Peng, G. Liu, K. McIlwrath, X. F. Zhang, R. A. Huggins and Y. Cui, *Nat. Nanotechnol.*, 2008, **3**, 31–35.
5 S. W. Lee, M. T. McDowell, J. W. Choi and Y. Cui, *Nano Lett.*, 2011, **11**, 3034–3039.

 

6 A. I. Hochbaum, R. Chen, R. D. Delgado, W. Liang, E. C. Garnett, M. Najarian, A. Majumdar and P. Yang, *Nature*, 2008, **451**, 163–167.
7 A. I. Boukai, Y. Bunimovich, J. Tahir-Kheli, J. K. Yu, W. A. Goddard 3rd and J. R. Heath, *Nature*, 2008, **451**, 168–171.
8 T. Zhang, S. L. Wu, R. T. Zheng and G. A. Cheng, *Nanotechnology*, 2013, **24**, 505718.
9 L. Hu and G. Chen, *Nano Lett.*, 2007, **7**, 3249–3252.
10 K. Q. Peng, X. Wang, L. Li, Y. Hu and S. T. Lee, *Nano Today*, 2013, **8**, 75–97.
11 K. Q. Peng and S. T. Lee, *Adv. Mater.*, 2011, **23**, 198–215.
12 Y. Wu, Y. Cui, L. Huynh, C. J. Barrelet, D. C. Bell and C. M. Lieber, *Nano Lett.*, 2004, **4**, 433–436.
13 Y. Cui, L. J. Lauhon, M. S. Gudiksen, J. Wang and C. M. Lieber, *Appl. Phys. Lett.*, 2001, **78**, 2214.
14 N. Wang, Y. F. Zhang, Y. H. Tang, C. S. Lee and S. T. Lee, *Appl. Phys. Lett.*, 1998, **73**, 3902.
15 Z. Huang, N. Geyer, P. Werner, J. de Boor and U. Gosele, *Adv. Mater.*, 2011, **23**, 285–308.
16 K. Peng, A. Lu, R. Zhang and S.-T. Lee, *Adv. Funct. Mater.*, 2008, **18**, 3026–3035.
17 S. L. Wu, L. Wen, G. A. Cheng, R. T. Zheng and X. L. Wu, *ACS Appl. Mater. Interfaces*, 2013, **5**, 4769–4776.
18 S. S. Iyer and Y. H. Xie, *Science*, 1993, **260**, 40–46.
19 A. I. Hochbaum, D. Gargas, Y. J. Hwang and P. Yang, *Nano Lett.*, 2009, **9**, 3550–3554.
20 D. Li, Y. Wu, P. Kim, L. Shi, P. Yang and A. Majumdar, *Appl. Phys. Lett.*, 2003, **83**, 2934.
21 S. W. Lee, M. T. McDowell, L. A. Berla, W. D. Nix and Y. Cui, *Proc. Natl. Acad. Sci. U. S. A.*, 2012, **109**, 4080–4085.
22 Z. Huang, X. Zhang, M. Reiche, L. Liu, W. Lee, T. Shimizu, S. Senz and U. Gösele, *Nano Lett.*, 2008, **8**, 3046–3051.
23 Y.-K. Choi, J. Zhu, J. Grunes, J. Bokor and G. A. Somorjai, *J. Phys. Chem. B*, 2003, **107**, 3340–3343.
24 W. Chen and H. Ahmed, *Appl. Phys. Lett.*, 1993, **63**, 1116.
25 W. Q. Xie, J. I. Oh and W. Z. Shen, *Nanotechnology*, 2011, **22**, 065704.
26 Y. Qu, L. Liao, Y. Li, H. Zhang, Y. Huang and X. Duan, *Nano Lett.*, 2009, **9**, 4539–4543.
27 W. K. To, C. H. Tsang, H. H. Li and Z. Huang, *Nano Lett.*, 2011, **11**, 5252–5258.
28 K. Peng, H. Fang, J. Hu, Y. Wu, J. Zhu, Y. Yan and S. Lee, *Chemistry*, 2006, **12**, 7942–7947.
29 M. Ge, J. Rong, X. Fang and C. Zhou, *Nano Lett.*, 2012, **12**, 2318–2323.
30 C. L. Lee, K. Tsujino, Y. Kanda, S. Ikeda and M. Matsumura, *J. Mater. Chem.*, 2008, **18**, 1015.